

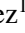
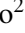


LETTER TO THE EDITOR

Discovery of the C_7N^- anion in TMC-1 and IRC +10216[★]

J. Cernicharo¹, J. R. Pardo¹ , C. Cabezas¹ , M. Agúndez¹ , B. Tercero^{2,3} , N. Marcelino², R. Fuentetaja¹,
M. Guélin⁴, and P. de Vicente³

¹ Grupo de Astrofísica Molecular, Instituto de Física Fundamental (IFF-CSIC), C/ Serrano 121, 28006 Madrid, Spain
e-mail: jose.cernicharo@csic.es

² Centro de Desarrollos Tecnológicos, Observatorio de Yebes (IGN), 19141 Yebes, Guadalajara, Spain

³ Observatorio Astronómico Nacional (OAN, IGN), Madrid, Spain

⁴ Institut de Radioastronomie Millimétrique, 300 rue de la Piscine, 38406 Saint Martin d'Hères, France

Received 29 December 2022 / Accepted 30 January 2023

ABSTRACT

We report on the discovery of the C_7N^- anion towards the starless core TMC-1 and towards the carbon-rich evolved star IRC +10216. We used the data of the QUIJOTE (*Q*-band Ultrasensitive Inspection Journey to the Obscure TMC-1 Environment) line survey towards TMC-1 and found six lines in perfect harmonic frequency relation from $J = 27 - 26$ up to $J = 32 - 31$. The frequency of the lines can be reproduced with a rotational constant and a distortion constant of $B = 582.68490 \pm 0.00024$ MHz and $D = 4.01 \pm 0.13$ Hz, respectively. The standard deviation of the fit is 4 kHz. Towards IRC +10216, we identify 17 lines from $J = 27 - 26$ up to $J = 43 - 42$; their frequencies are also in harmonic relation, providing $B = 582.6827 \pm 0.00085$ MHz and $D = 3.31 \pm 0.31$ Hz. The nearly exact coincidence of the rotational and distortion constants in both sources points unambiguously to a common molecular carrier. Taking into account the chemical peculiarities of both sources, the carrier could be a radical or an anion. The radical can be discarded, as the observed lines belong to a singlet species. Hence, the most plausible carrier is an anion. High-level ab initio calculations indicate that C_7N^- , for which we compute a rotational constant of $B = 582.0$ MHz and a dipole moment of 7.5 D, is the carrier of the lines in both sources. We predict the neutral C_7N to have a ground electronic state $^2\Pi$ and a dipole moment of ~ 1 D. Because of this low value of μ and to its much larger rotational partition function, its lines are expected to be well below the sensitivity of our data for both sources.

Key words. molecular data – line: identification – ISM: molecules – ISM: individual objects: TMC-1 – ISM: individual objects: IRC+10216 – astrochemistry

1. Introduction

The presence of carbon-chain negative ions in space was predicted on the grounds that electron radiative attachment is efficient for open-shell molecules with large electron affinities (Dalgarno & McCray 1973; Sarre 1980; Herbst 1981). The predicted abundance ratio between an anion and its corresponding neutral species increases with the size of the molecule, which is a consequence of the increasing density of vibrational states as the number of atoms in the molecule increases.

The first anion detected in space, C_6H^- , was observed towards TMC-1 (McCarthy et al. 2006). Lines from this species were already reported as unidentified features in the line survey of IRC +10216 performed with the Nobeyama 45m telescope by Kawaguchi et al. (1995). Aoki (2000) suggested that the carrier of these lines was C_6H^- from ab initio calculations, which was finally confirmed by the laboratory observations of McCarthy et al. (2006). The presence of this anion in space attracted significant attention and motivated searches for other hydrocarbon anions in interstellar and circumstellar clouds. C_4H^- was first discovered in the circumstellar cloud IRC +10216 by Cernicharo et al. (2007) and then in the interstel-

lar clouds L1527, Lupus-1A, and TMC-1 (Agúndez et al. 2008; Sakai et al. 2008, 2010; Cordiner et al. 2013). Following the observation of C_8H^- in the laboratory (Gupta et al. 2007), this anion was found in TMC-1 (Brünken et al. 2007), IRC +10216 (Kawaguchi et al. 2007; Remijan et al. 2007), and Lupus-1A (Sakai et al. 2010). Remijan et al. (2023) recently announced the detection of $C_{10}H^-$ in TMC-1. Although we searched for it and other anions, we cannot confirm any line of this species in the QUIJOTE¹ line survey, probably due to the high- J levels involved in the rotational transitions of $C_{10}H^-$ in our data ($J_u \geq 52$ and $E_u > 40$ K).

The nitrile anions CN^- , C_3N^- , and C_5N^- were first detected in the circumstellar envelope of the carbon-rich star IRC +10216 (Agúndez et al. 2010; Thaddeus et al. 2008; Cernicharo et al. 2008, 2020). CN^- and C_3N^- were detected thanks to accurate laboratory frequencies (Gottlieb et al. 2007; Thaddeus et al. 2008; Amano 2008). However, the assignment of C_5N^- was based on ab initio calculations by Botschwina & Oswald (2008) and Aoki (2000). Although C_5N^- was the best candidate, the lack of precise laboratory frequencies prevented metal-bearing molecules being ruled out, such as MgC_3N and MgC_4H . Later on, these two molecules were identified in IRC +10216 based on ab initio calculations (Cernicharo et al. 2019). Moreover,

[★] Based on observations carried out with the Yebes 40m telescope (projects 19A003, 20A014, 20D023, and 21A011). The 40m radiotelescope at Yebes Observatory is operated by the Spanish Geographic Institute (IGN, Ministerio de Transportes, Movilidad y Agenda Urbana).

¹ *Q*-band Ultrasensitive Inspection Journey to the Obscure TMC-1 Environment.

a series of lines with the same rotational constant as that assigned to C_5N^- in IRC+10216 were recently observed in TMC-1 (Cernicharo et al. 2020), which ruled out metal-bearing molecules and provided strong support in favour of C_5N^- .

There is controversy over the formation of C_nN^- anions through radiative electron attachment to C_nN radicals because calculated rate coefficients can differ by orders of magnitude depending on the study (Petrie & Herbst 1997; Walsh et al. 2009; Khamesian et al. 2016; Millar et al. 2017). Hence, the detection of nitrile anions and the determination of their abundances in different astronomical environments are an important step forward in understanding the chemistry of anions in space.

In this Letter, we present the discovery of C_7N^- in the cold dark core TMC-1 and in the external layers of the circumstellar envelope of the carbon-rich star IRC+10216. The assignment is based on the excellent agreement between the derived rotational constant and that from high-level ab initio calculations performed in this work (see also Botschwina & Oswald 2008). The assignment to C_7N^- is strengthened by the lack of other plausible candidates common to both sources.

2. Observations

New receivers built within the Nanocosmos² project and installed at the Yebes 40m radiotelescope were used for observations of TMC-1 ($\alpha_{J2000} = 4^h41^m41.9^s$ and $\delta_{J2000} = +25^\circ41'27.0''$) and IRC+10216 ($\alpha_{J2000} = 9^h47^m57.36^s$ and $\delta_{J2000} = +13^\circ16'44.4''$). The observations of TMC-1 belong to the QUIJOTE line survey (Cernicharo et al. 2021) and those of IRC+10216 to the Nanocosmos² survey of evolved stars (Pardo et al. 2022). A detailed description of the telescope, receivers, and backends is given by Tercero et al. (2021). Briefly, the receiver consists of two cold, high-electron-mobility transistor amplifiers covering the 31.0–50.3 GHz band with horizontal and vertical polarisations. Receiver temperatures in the runs achieved during 2020 vary from 22 K at 32 GHz to 42 K at 50 GHz. Some power adaptation in the down-conversion chains reduced the receiver temperatures during 2021 to 16 K at 32 GHz and 25 K at 50 GHz. The backends are $2 \times 8 \times 2.5$ GHz fast Fourier transform spectrometers with a spectral resolution of 38.15 kHz, providing coverage of the whole Q -band in both polarisations. For the observations of TMC-1, the original spectral resolution was used, while for IRC+10216, the data have been smoothed to 220 kHz, which corresponds to a velocity resolution of 1.7 km s^{-1} at 40 GHz. This resolution is large enough to resolve the U-shaped lines of IRC+10216, which exhibit a full velocity width of 29 km s^{-1} (Cernicharo et al. 2000).

All observations of TMC-1 were performed in the frequency switching mode with frequency throws of 8 and 10 MHz. Details of the survey and the data-analysis procedure are given in Cernicharo et al. (2021, 2022). The observations of IRC+10216 were performed in position switching and are described by Pardo et al. (2022). The main beam efficiency of the telescope varies from 0.6 at 32 GHz to 0.43 at 50 GHz. The intensity scale used in this work, namely antenna temperature (T_A^*), was calibrated using two absorbers at different temperatures and the atmospheric transmission model ATM (Cernicharo 1985; Pardo et al. 2001). Calibration uncertainties of 10% are adopted. However, some systematic effects were observed between the data acquired during 2022 and 2021. The intensity of the lines in the earliest observations of QUIJOTE are typically 10%–15%

weaker than those of the most recent observations. No frequency effects are observed in the derived calibration factors. This systematic change is probably related to the surface adjustment after holography measurements at the end of 2021. The whole set of data has been recalibrated and co-added to produce the QUIJOTE line survey used for this work. The new line intensities, and hence the column densities, are $\sim 15\%$ larger than those previously reported. The data for TMC-1 and IRC+10216 presented here correspond to 758 h and 696 h of on-source telescope time, respectively. All data were analysed using the GILDAS package³.

3. Detection of C_7N^-

Line identification in this work was done using the catalogues MADEX (Cernicharo 2012), CDMS (Müller et al. 2005), and JPL (Pickett et al. 1998). By November 2022, the MADEX code contained 6446 spectral entries corresponding to the ground and vibrationally excited states –together with the corresponding isotopologues– of 1746 molecules.

The new data of IRC+10216 have an unprecedented sensitivity of 0.1 mK in the T_A^* scale and for a spectral resolution of 220 kHz, and the survey shows a forest of unidentified lines. A series of doublets and triplets are found in very good harmonic relation at slightly higher frequencies than the rotational lines of HC_9N ; their rotational constants are around 291 MHz. These results will be reported in a forthcoming paper (Pardo et al., in prep.). These lines correspond to the $\nu_{19} = 2, 3$ vibrational levels of HC_9N . Their quantum numbers go from $J_u = 54$ up to $J_u = 80$. Some of them are shown in Fig. 1. In addition, we find that an extra line was detected every two transitions of the $HC_9N \nu_{19} = 2$ transitions following a perfect harmonic relation from $J = 27 - 26$ up to $J = 42 - 43$ with a rotational constant of $B = 582.6$ MHz. The possibility that these lines also belong to a vibrational excited state of HC_9N is immediately ruled out because if B were 291.3, then all lines with odd J_u would be missing. The lines are shown in Fig. 1 and appear as single features; the carrier is therefore a $^1\Sigma$ molecule, or a $^2\Sigma$ molecule with a very small value of γ . A fit to the observed lines provides the rotational and distortion constants given in Table 1. Taking into account the observed line profile of the unblended lines, the carrier has to be produced in the external layers of the circumstellar envelope of IRC+10216, that is, in the region where chemistry is controlled by the Galactic UV photons and where radicals, cyanopolynes, carbon chains, metal-bearing species, and anions are detected (see e.g. Cernicharo et al. 2000).

In order to obtain additional insight into the carrier of the lines we checked if they are present in the QUIJOTE line survey of TMC-1. Six of them are clearly detected, corresponding to the transitions $J = 27 - 26$ up to $J = 32 - 31$. These are shown in Fig. 2. None of them show signs of fine or hyperfine structure and they therefore definitively belong to a $^1\Sigma$ molecule. The rotational and distortion constant are given in Table 1 and agree very well with those derived from the 17 lines of IRC+10216. Moreover, the common measured frequencies in both sources are identical within the measured uncertainties for the IRC+10216 lines. The carrier is therefore common to both sources and consequently we can exclude a metal-bearing species or a vibrationally excited state as these are not expected in TMC-1. As we find no evidence of fine structure, we can also discard a radical as the carrier. Moreover, we can also discard an isotopologue of an abundant species such as HC_7N for which $B = 564$ MHz,

² ERC grant ERC-2013-Syg-610256-NANOCOSMOS.
<https://nanocosmos.iff.csic.es/>

³ <http://www.iram.fr/IRAMFR/GILDAS>

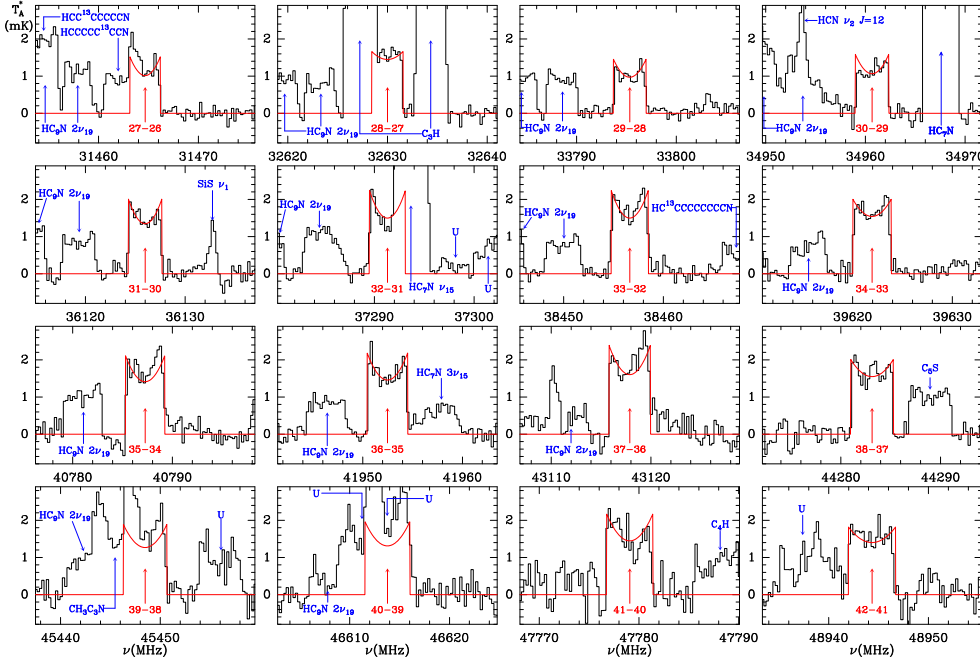


Fig. 1. Observed lines of C_7N^- towards IRC +10216. Line parameters are given in Table A.1. The abscissa corresponds to the rest frequency assuming a local standard of rest velocity of -26.5 km s^{-1} . The ordinate is the antenna temperature corrected for atmospheric and telescope losses in milliKelvin. The red lines show the fitted line profiles.

Table 1. Rotational and distortion constants for C_7N^- .

	TMC-1 ^(a)	IRC +10216 ^(b)	All data ^(c)	Ab initio ^(d)
B (MHz)	582.68492 ± 0.00024	582.68274 ± 0.00085	582.68490 ± 0.00022	582.75
D (Hz)	4.01 ± 0.13	3.31 ± 0.31	4.00 ± 0.12	4.3
N_{lines}	6	17	17	
J_{max}	32	43	43	
σ (kHz)	4.0	61	43	

Notes. ^(a)Parameters derived using the frequencies measured towards TMC-1 (see Table A.2). ^(b)Parameters derived using the frequencies measured towards IRC +10216 (see Table A.1). ^(c)Parameters derived using the frequencies of the lines $J = 27 - 26$ up to $J = 32 - 31$ measured in TMC-1, and $J = 33 - 32$ up to $J = 43 - 42$ measured in IRC +10216. ^(d)Computed rotational constant from ab initio calculations as described in the text (see also Botschwina & Oswald 2008).

and C_8H for which B is 587.264 MHz (McCarthy et al. 1999). An isotopologue of C_8H can be discarded due to the fact that the carrier has to be a singlet state. The rotational constants of the isotopologues of HC_7N have been measured in the laboratory (McCarthy et al. 2000) and all them have rotational constants below that of the carrier. Hence, we have to conclude that we are dealing with a new unknown molecular species. Nevertheless, its structure has to be similar to that of HC_7N and C_8H . An isomer of HC_7N can be excluded as HC_6NC , the most likely candidate, has been observed in the laboratory to have a rotational constant of 582.5203 MHz (Botschwina et al. 1998) and is not detected in either TMC-1 or IRC+10216. The other isomers, HC_xNC_{7-x} , are expected to have larger rotational constants, except HNC_7 for which the expected rotational constant is around 567 MHz (da Silva & Neto 1997; Lee et al. 2000). Therefore, the most plausible candidates are C_7N and C_7N^- . The former can be discarded as its ground electronic state is predicted to be 2Π with a 2Σ state close in energy (Botschwina et al. 1999). This leaves the anion C_7N^- as the most likely carrier of the lines in TMC-1 and IRC +10216. Lines of the previous member of the series, C_5N^- , have been found in both sources (Cernicharo et al. 2008, 2020). Ab initio calculations by Botschwina & Oswald (2008) indicate a rotational constant for this anion of 582 MHz, very close indeed to the observed value, and a dipole moment of 7.545 D.

We performed geometry ab initio calculations (Werner et al. 2020) using the coupled cluster method with single, double, and perturbative triple excitations with an explicitly correlated approximation (CCSD(T)-F12; Knizia et al. 2009) and all electrons (valence and core) correlated together with the Dunning's correlation consistent basis sets with polarized core-valence correlation triple- ζ for explicitly correlated calculations (cc-pCVTZ; Hill et al. 2010). The values for the centrifugal distortion constant were calculated (Frisch et al. 2016) using the MP2 perturbation theory method (Møller & Plesset 1934) and the correlation is consistent with polarized valence triple- ζ basis set (cc-pVTZ; Woon & Dunning 1993). The values of B and D calculated for C_7N^- were scaled by the corresponding experimental and calculated ratios obtained for HC_7N using the same level of theory. For HC_7N , we obtained $B = 562.9$ MHz and $D = 3.50$ Hz, while for C_7N^- the uncorrected values are $B = 581.6$ MHz and $D = 3.70$ Hz. The scaled values for C_7N^- are presented in Table 1 and perfectly match those measured for the lines in TMC-1 and IRC +10216.

We therefore conclude that we have discovered the C_7N^- anion in the interstellar and circumstellar media. A fit to the lines observed in both sources provides $B = 582.68495 \pm 0.0024$ MHz and $D = 4.02 \pm 0.13$ Hz (see Table 1), which are the recommended rotational parameters with which to predict the spectrum of C_7N^- .

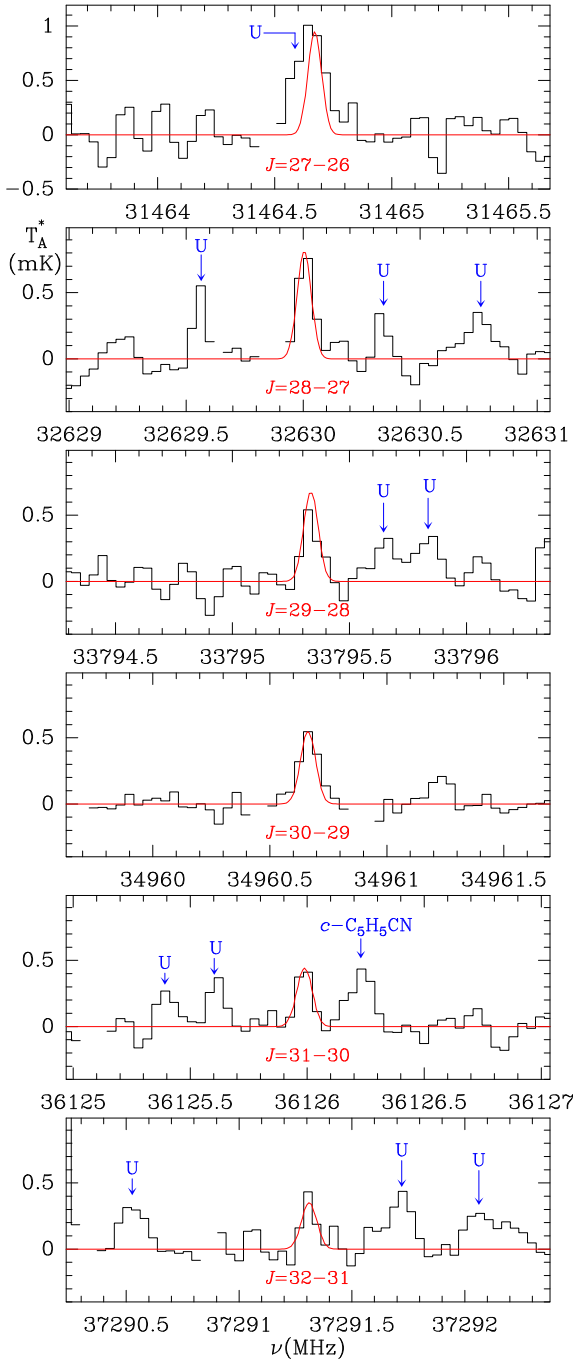


Fig. 2. Observed lines of C_7N^- towards TMC-1. Line parameters are given in Table A.2. The abscissa corresponds to the rest frequency assuming a local standard of rest velocity of $+5.83 \text{ km s}^{-1}$. The ordinate is the antenna temperature corrected for atmospheric and telescope losses in milliKelvin. The red line shows the synthetic spectrum derived for $T_{\text{rot}} = 6 \text{ K}$ and $N(C_7N^-) = 5 \times 10^{10} \text{ cm}^{-2}$. Blank channels correspond to negative features produced in the folding of the frequency-switching data.

4. Discussion

Assuming a source emission diameter of $80''$ for C_7N^- in TMC-1 (Fossé et al. 2001), a fit to the observed line profiles results in a rotational temperature of $6.0 \pm 0.5 \text{ K}$ and a column density of $(5.0 \pm 0.5) \times 10^{10} \text{ cm}^{-2}$. Adopting an averaged column density of H_2 over the source of 10^{22} cm^{-2} (Cernicharo et al. 1987), the abundance of C_7N^- is 5×10^{-12} . The column density of C_5N^- in

TMC-1 is $(2.6 \pm 0.9) \times 10^{11} \text{ cm}^{-2}$ (Cernicharo et al. 2020), and therefore the abundance ratio C_5N^-/C_7N^- is ~ 5 . However, we note that due to the high energy of the rotational levels associated to the observed transitions, small variations of the rotational temperature can be compensated by a significant variation of the column density with a negligible variation of χ^2 . This means that, in light of the lack of information regarding the intensity of low- J transitions, T_{rot} and N are strongly correlated.

For IRC+10216, we assume that the emitting region has a radius of $15''$, which corresponds to the observed spatial distribution of cyanopolyynes and radicals with ALMA (Agúndez et al. 2017). A rotation diagram of the observed intensities towards IRC+10216 provides a rotational temperature of $26.6 \pm 1.8 \text{ K}$ and a column density of $(2.4 \pm 0.2) \times 10^{12} \text{ cm}^{-2}$ for C_7N^- . The column density of C_5N^- was previously derived in this source from lines observed at 3 mm to be $3.4 \times 10^{12} \text{ cm}^{-2}$ (Cernicharo et al. 2008). However, several lines of C_5N^- have been observed in the Q -band in our survey with the Yebes 40m telescope and those at 3 mm observed with the IRAM 30m telescope have been significantly improved (Cernicharo et al. 2020). From all these data, we derived a column density of C_5N^- in IRC+10216 from a rotation diagram analysis, which provides $N(C_5N^-) = (5.7 \pm 0.3) \times 10^{12} \text{ cm}^{-2}$ and $T_{\text{rot}} = 29.9 \pm 0.6 \text{ K}$. The C_5N^-/C_7N^- abundance ratio is therefore ~ 2.4 , which is similar to that found in TMC-1.

The detection of C_7N^- in interstellar and circumstellar environments implies that C_7N must also be present in both media if the anion is formed via electron attachment to the radical. For the neutral species C_7N , ab initio calculations by Botschwina et al. (1999) predict an electronic ground state $^2\Pi$ with a moderate dipole moment of ~ 1 . However, due to the possible admixing of the ground state with a low-lying $^2\Sigma$ state, which has a dipole moment of ~ 3.6 (Botschwina et al. 1999), the real value of the dipole moment could be between those of both states. This mixing of two low-lying electronic states was previously discussed for C_5N (Cernicharo et al. 2008) and C_4H (Oyama et al. 2020). Taking into account the observed intensities of C_7N^- ($\mu = 7.545 \text{ D}$) in TMC-1 and IRC+10216, those of C_7N could be much lower due to the lower dipole moment of the neutral and to the larger partition function of the radical caused by the presence of two ladders, $^2\Pi_{1/2}$ and $^2\Pi_{3/2}$, each one exhibiting Λ -doubling and hyperfine structure. Adopting an averaged dipole for C_7N of between those of the $^2\Pi$ and $^2\Sigma$ states of 2.3 D (Botschwina et al. 1999) and a rotational partition function four times larger than for C_7N^- , the lines of the radical could be $\sim 40 \times N(C_7N^-)/N(C_7N)$ times weaker than those of C_7N^- . Adopting a $N(C_7N^-)/N(C_7N)$ similar to the $N(C_5N^-)/N(C_5N)$, which is found to be ~ 0.5 in IRC+10216 and TMC-1 (Cernicharo et al. 2008, 2020), the expected intensities will be approximately 20 times weaker for C_7N than for C_7N^- , which is well below the present sensitivity of our data towards the two sources. We can also make a prediction of the expected intensities of C_7N based on those of the analogue radical C_8H , which has a similar partition function to C_7N (excluding the hyperfine structure), although a larger dipole moment of 6.5 D . The lines of C_7N will have an intensity of $N(C_7N)/N(C_8H) \times [(\mu(C_7N)/\mu(C_8H))]^2$ times those of C_8H ; that is, $\sim N(C_7N)/N(C_8H)/8$. The lines of the $^2\Pi_{3/2}$ ladder of C_8H have an intensity of $\sim 5 \text{ mK}$ in TMC-1 and of 4 mK in IRC+10216 at 31 GHz . Therefore, detecting C_7N in our data will require an abundance for this species of similar to or larger than that of C_8H , which is very unlikely in view of the observed abundance ratios of other members of these two families of radicals. For example, the abundance ratios C_3N/C_4H and

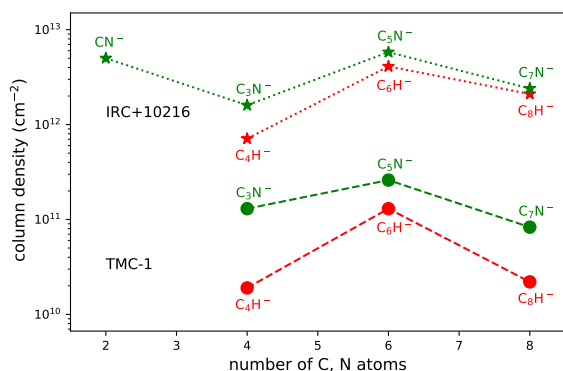


Fig. 3. Column densities of negative ions derived through observations toward TMC-1 and IRC +10216. Values are taken from this work, from Agúndez et al., (in prep.), and from the literature (Cernicharo et al. 2007, 2020; Remijan et al. 2007; Thaddeus et al. 2008; Agúndez et al. 2008, 2010).

C₅N/C₆H are on the order of 0.1 in both IRC +10216 and TMC-1 (Cernicharo et al. 2000; Agúndez & Wakelam 2013).

The detection of C₇N⁻ is in line with previous observational constraints of the series of hydrocarbon and nitrile anions C_nH⁻ and C_nN⁻ in which long carbon chains are favoured with respect to the short ones. Although we do not have access to the C₇N⁻/C₇N abundance ratio, we expect this ratio to be in the range of 0.1–0.5, as found for other large anions, such as C₈H⁻ and C₅N⁻ (Cernicharo et al. 2008, 2020; Brünken et al. 2007; Remijan et al. 2007). This scenario is in agreement with the proposed formation mechanism of negative ions from electron attachment to the corresponding radical (Herbst 1981), which becomes increasingly efficient as the size of the chain increases, as calculated for the series of hydrocarbon radicals C_nH (Herbst & Osamura 2008). It would be interesting to compute the rate coefficient of electron attachment for the series of nitrile radicals C_nN. Calculated values for C₃N (Petrie & Herbst 1997; Harada & Herbst 2008) and C₅N (Walsh et al. 2009) indicate that, similarly to the case of hydrocarbons, the rate coefficient increases considerably as the size of the chain increases, although Khamesian et al. (2016) find much lower rate coefficients for C₃N and C₅N.

It is interesting to note that, although the anion-to-neutral ratio increases considerably with increasing chain length, the column densities of negative ions are on the same order along the series of hydrocarbons C_nH⁻ and nitriles C_nN⁻ (see Fig. 3). This is interesting because if this behaviour is maintained for larger sizes, we could expect the anions C₁₀H⁻ and C₉N⁻ to be present in significant amounts, allowing their detection in TMC-1 and IRC +10216 at centimetre wavelengths. Moreover, looking at anions would allow us to probe the extent to which carbon chains can grow, and this would be more straightforward than looking at neutrals. This is due to the fact that, for large carbon chains, the detection of the anion is favoured over the radical because of the collapse of the fine and hyperfine structure and eventually also because of the more favourable dipole moment, as perfectly illustrated in the case of C₇N⁻ and C₇N.

5. Conclusions

We report in this work the detection of the anion C₇N⁻ in TMC-1 and IRC +10216. The lack of detection of the neutral C₇N is due to its much lower dipole moment and larger partition function.

Acknowledgements. We thank ERC for funding through grant ERC-2013-SyG-610256-NANOCOSMOS. M.A. thanks MICIU for grant RyC-2014-16277. We also thank Ministerio de Ciencia e Innovación of Spain (MICIU) for funding support through projects PID2019-106110GB-I00, PID2019-107115GB-C21/AEI/10.13039/501100011033, and PID2019-106235GB-I00.

References

- Agúndez, M., & Wakelam, V. 2013, *Chem. Rev.*, **113**, 8710
 Agúndez, M., Cernicharo, J., Guélin, M., et al. 2008, *A&A*, **478**, L19
 Agúndez, M., Cernicharo, J., Guélin, M., et al. 2010, *A&A*, **517**, L2
 Agúndez, M., Cernicharo, J., Quintana-Lacaci, G., et al. 2017, *A&A*, **601**, A4
 Amano, T. 2008, *J. Chem. Phys.*, **129**, 244305
 Aoki, K. 2000, *Chem. Phys. Lett.*, **323**, 55
 Botschwina, P., & Oswald, R. 2008, *J. Chem. Phys.*, **129**, 044305
 Botschwina, P., Heyl, A., Chen, W., et al. 1998, *J. Chem. Phys.*, **109**, 3108
 Botschwina, P., Horn, M., Markey, K., & Oswald, R. 1999, *Mol. Phys.*, **92**, 3
 Brünken, S., Gupta, H., Gottlieb, C. A., et al. 2007, *ApJ*, **664**, L43
 Cernicharo, J. 1985, *Internal IRAM Report* (Granada: IRAM)
 Cernicharo, J. 2012, in *ECLA 2011: Proc. of the European Conference on Laboratory Astrophysics*, eds. C. Stehl, C. Joblin, & L. d'Hendecourt (Cambridge: Cambridge Univ. Press), *EAS Publ. Ser.*, **2012**, 251
 Cernicharo, J., Guélin, M., & Walmsley, C. M. 1987, *A&A*, **172**, L5
 Cernicharo, J., Guélin, M., & Kahane, C. 2000, *A&AS*, **142**, 181
 Cernicharo, J., Guélin, M., Agúndez, M., et al. 2007, *A&A*, **467**, L37
 Cernicharo, J., Guélin, M., Agúndez, M., et al. 2008, *ApJ*, **688**, L83
 Cernicharo, J., Cabezas, C., Pardo, J. R., et al. 2019, *A&A*, **630**, L2
 Cernicharo, J., Marcelino, N., Pardo, J. R., et al. 2020, *A&A*, **641**, L9
 Cernicharo, J., Agúndez, M., Kaiser, R., et al. 2021, *A&A*, **652**, L9
 Cernicharo, J., Fuentetaja, R., Agúndez, M., et al. 2022, *A&A*, **663**, L9
 Cordiner, M. A., Buckle, J. V., Wirstrom, E. S., et al. 2013, *ApJ*, **770**, 48
 Dalgarno, A., & McCray, R. A. 1973, *ApJ*, **181**, 95
 da Silva, J. B. P., Neto, B. B., & Ramos, M.N., 1997, *J. Mol. Struct.*, **389**, 279
 Fossé, D., Cernicharo, J., Gerin, M., & Cox, P. 2001, *ApJ*, **552**, 168
 Frisch, M. J., Trucks, G. W., Schlegel, H. B., et al. 2016, *Gaussian 16 Revision A.03*
 Gottlieb, C. A., Brünken, S., McCarthy, M. C., & Thaddeus, P. 2007, *J. Chem. Phys.*, **126**, 191101
 Gupta, H., Brünken, S., Tamassia, F., et al. 2007, *ApJ*, **655**, L57
 Gupta, H., Gottlieb, C. A., McCarthy, M. C., & Thaddeus, P. 2009, *ApJ*, **691**, 1494
 Harada, N., & Herbst, E. 2008, *ApJ*, **685**, 272
 Herbst, E. 1981, *Nature*, **289**, 656
 Herbst, E., & Osamura, Y. 2008, *ApJ*, **679**, 1670
 Hill, J. G., Mazumder, S., & Peterson, K. A. 2010, *J. Chem. Phys.*, **132**
 Knizia, G., Adler, T. B., & Werner, H.-J. 2009, *J. Chem. Phys.*, **130**
 Kawaguchi, K., Kasai, Y., Ishikawa, S., & Kaifu, N. 1995, *PASJ*, **47**, 853
 Kawaguchi, K., Fujimori, R., & Aimi, S. 2007, *PASJ*, **59**, L47
 Khamesian, M., Douguet, N., Fonseca, S., et al. 2016, *Phys. Rev. Lett.*, **117**, 123001
 Lee, S.-C., Park, S.-W., & Lee, S. 2000, *Bull. Korean Chem. Soc.*, **21**, 734
 McCarthy, M. C., Chen, W., Apponi, A. J., et al. 1999, *ApJ*, **520**, 158
 McCarthy, M. C., Levine, E. S., Apponi, A. J., & Thaddeus, P. 2000, *J. Mol. Spectrosc.*, **203**, 75
 McCarthy, M. C., Gottlieb, C. A., Gupta, H. C., et al. 2006, *ApJ*, **652**, L141
 Millar, T. J., Walsh, C., & Field, T. A. 2017, *Chem. Rev.*, **117**, 1765
 Møller, C., & Plesset, M. S. 1934, *Phys. Rev.*, **46**, 618
 Müller, H. S. P., Schlöder, F., Stutzki, J., & Winnewisser, G. 2005, *J. Mol. Struct.*, **742**, 215
 Oyama, T., Ozaki, H., Sumiyoshi, Y., et al. 2020, *ApJ*, **890**, 39
 Petrie, S., & Herbst, E. 1997, *ApJ*, **491**, 210
 Pardo, J. R., Cernicharo, J., & Serabyn, E. 2001, *IEEE Trans. Antennas and Propagation*, **49**, 12
 Pardo, J. R., Cernicharo, J., Tercero, B., et al. 2022, *A&A*, **658**, A39
 Pickett, H. M., Poynter, R. L., Cohen, E. A., et al. 1998, *J. Quant. Spectrosc. Radiat. Trans.*, **60**, 883
 Remijan, A. J., Hollis, J. M., Lovas, F. J., et al. 2007, *ApJ*, **664**, L47
 Remijan, A. J., Scolati, H. N., Burkhardt, A. M., et al. 2023, *ArXiv eprints [arXiv:2301.07760]*
 Sakai, N., Sakai, T., & Yamamoto, S. 2008, *ApJ*, **673**, L71
 Sakai, N., Shiino, T., Hirota, T., et al. 2010, *ApJ*, **718**, L49
 Sarre, P. J. 1980, *J. Chem. Phys.*, **77**, 769
 Tercero, F., López-Pérez, J. A., Gallego, J., et al. 2021, *A&A*, **645**, A37
 Thaddeus, P., Gottlieb, C. A., Gupta, H., et al. 2008, *ApJ*, **677**, 1132
 Walsh, C., Harada, N., Herbst, E., & Millar, T. J. 2009, *ApJ*, **700**, 752
 Werner, H. J., Knowles, P. J., Knizia, G., et al. 2020, *MOLPRO, version 2020.2*
 Woon, D. E., & Dunning, T. H., Jr 1993, *J. Chem. Phys.*, **98**, 1358

Appendix A: Line parameters

Line parameters for TMC-1 were obtained by fitting a Gaussian line profile to the observed data. A window of $\pm 15 \text{ km s}^{-1}$ around the v_{LSR} of the source was considered for each transition. The derived line parameters are given in Table A.2.

For IRC +10216, we used the SHELL method of the GILDAS³ package which is well adapted to reproducing the observed line profiles in circumstellar envelopes. A variable window of 50-100 MHz was used to derive the line parameters in this source; these are given in Table A.1.

Table A.1. Observed lines of C_7N^- in IRC +10216.

Transition	ν_{obs}^a	$\nu_{obs} - \nu_{cal}^b$	$\int T_A^* dv^c$	$T_A^*(horn)^d$	$T_A^*(center)^e$	σ^f	Notes
27-26	31464.50±0.10	-0.11	34.51±0.35	1.52	1.01		A
28-27	32630.00±0.10	0.05	43.94±0.44	1.66	1.44		B
29-28	33795.30±0.10	0.02	32.93±0.33	1.45	0.97		
30-29	34960.61±0.10	0.00	35.80±0.36	1.58	1.06		
31-30	36125.90±0.10	-0.04	43.85±0.44	2.00	1.35		
32-31	37291.34±0.10	0.07	50.66±0.50	2.25	1.50		C
33-32	38456.60±0.10	0.01	50.64±0.51	2.24	1.50		
34-33	39621.88±0.10	-0.02	49.44±0.49	2.00	1.54		
35-34	40787.30±0.10	0.07	47.66±0.48	2.11	1.41		
36-35	41952.50±0.10	-0.04	49.49±0.49	2.18	1.46		
37-36	43117.90±0.10	0.05	54.01±0.54	2.39	1.60		
38-37	44283.10±0.10	-0.06	49.51±0.50	2.01	1.55		
39-38	45448.50±0.10	0.03	42.65±0.43	1.89	1.27		D
40-39	46613.73±0.10	-0.04	44.39±0.44	1.96	1.31		E
41-40	47779.10±0.10	0.03	49.21±0.49	2.17	1.45		
42-41	48944.30±0.10	-0.07	44.66±0.45	1.82	1.40		
43-42	50109.70±0.10	0.04	43.83±13.0	1.78	1.37		F

Notes. ^aObserved frequency assuming a v_{LSR} of -26.5 km s^{-1} . ^bObserved minus calculated frequencies in MHz. ^cIntegrated line intensity in mK km s^{-1} . Uncertainty is assumed to be dominated by the calibration uncertainty of 10%. This uncertainty has been multiplied by a factor of 3 for the $J=43-42$ transition due to the poor atmospheric transmission at 50.1 GHz. ^dAntenna temperature at the terminal velocity (horn) in milli Kelvin. ^eAntenna temperature at line center in milli Kelvin. ^fRoot mean square noise of the data. ^ABlended with $\text{HCCCCC}^{13}\text{CCN}$. Line parameters can be still fitted. ^BBlended with C_3H . Line parameters can be still fitted. ^CBlended with $\text{HC}_7\text{N } v_{15}$. Line parameters can be still fitted. ^DBlended with $\text{CH}_3\text{C}_3\text{N}$. Line parameters can be still fitted. ^EBlended with a U feature. Line parameters very uncertain. ^FCalibration very uncertain.

Table A.2. Observed lines of C_7N^- in TMC-1.

Transition	ν_{obs}^a	$\nu_{obs} - \nu_{cal}^b$	$\int T_A^* dv^c$	Δv^d	$T_A^*^e$	σ^f
27-26	31464.665±0.020	-5.0	0.78±0.09	0.80±0.20	0.97	0.12 ^g
28-27	32630.005±0.010	1.5	0.65±0.08	0.76±0.05	0.80	0.10
29-28	33795.331±0.010	-3.3	0.40±0.09	0.71±0.18	0.52	0.11
30-29	34960.667±0.010	4.8	0.49±0.05	0.90±0.12	0.53	0.08
31-30	36125.987±0.010	-0.3	0.31±0.06	0.61±0.15	0.48	0.09
32-31	37291.308±0.020	-1.5	0.24±0.05	0.53±0.11	0.44	0.09
33-32	38456.628±0.004					$\leq 0.24^h$

Notes. ^aObserved frequency assuming a v_{LSR} of 5.83 km s^{-1} . ^bObserved minus calculated frequencies in kHz. ^cIntegrated line intensity in mK km s^{-1} . ^dLine width at half intensity derived by fitting a Gaussian function to the observed line profile (in km s^{-1}). ^eAntenna temperature in milliKelvin. ^fRoot mean square noise of the data. ^gLine blended with a U feature at 31464.59 MHz. ^h 3σ upper limit. The frequency of this transition corresponds to the predicted one from the constants given in Table 1.